Index Terms

noise reduction, DTCWT, shrinkage, random sprays, image enhancement.

Noise reduction based on partial-reference, dual-tree complex wavelet transform shrinkage

Massimo Fierro, Ho-Gun Ha,Yeong-Ho Ha, *Senior Member, IEEE,*

Abstract

This work presents a novel way to reduce point-wise noise introduced or exacerbated by image enhancement methods, in particular algorithms based on the random spray sampling technique. According to the nature of the sprays, the output images of such methods tend to exhibit noise with an unknown distribution. The proposed noise reduction method is based on the assumption that the non-enhanced image is either free of noise or contaminated by non-perceivable levels of noise. The dual-tree complex wavelet transform is applied to the luma channel of both the non-enhanced and enhanced image. The standard deviation of the energy for the non-enhanced imageis computed across the six orientations and normalized. The resulting normalized map is used to shrink the real coefficients of the enhanced image decomposition. A noise-reduced version of the enhanced image can then be computed via the inverse transforms. A thorough numerical analysis of the results has been performed in order to confirm the validity of the proposed approach.

I. Introduction

Although the field of image enhancement has been active since before digital imagery achieved a consumer status, it has never stopped evolving. Therefore, the present work introduces a novel multi-resolution denoising method, tailored to address a specific image quality problem expressed by some image enhancement algorithms. While inspired by the peculiar problem of Random Spray based image enhancement methods, it should be noted that the proposed noise reduction approach also works for other image enhancement processes that either introduce or exacerbate point-wise noise.

Sprays are a two-dimensional collection of points (coordinates) with a given spatial distribution around the origin that can be scaled and translated to sample an image support in a similar way to that employed by the Human Visual System (HVS). However, due to the peaked nature of sprays, undersired noise is

All the authors are with the School of Electronics Engineering, Kyungpook National University, Daegu, 702-701 Korea

often introduced in the output images generated by image enhancement algorithms that use sprays as image scanning structures. The amount and statistical characteristics of such noise depend on several factors, including image content and spray properties.

Multi-resolution, transform space denoising methods have along history. A particular branch is that reducing the magnitude of the transform coefficients according to certain criteria. Such an approach is often referred to as *shrinkage*. Some of the most commonly used transforms for shrinkage-based noise reduction are the Wavelet Transform (WT) [1]–[3], the Steerable Pyramid Transform [4]–[6], the Contourlet Transform [7]–[9] and the Shearlet Transform [10]–[12]. With the exception of the WT, all other transforms lead to over-complete data representations. Over-completeness is an important characteristic, as it is usually associated with the ability to distinguish data directionality in the transform space.

Independent of the specific transform used. the general assumption in multi-resolution shrinkage is that image data gives rise to sparse coefficients in the transform space. Thus, denoising can be achieved by compressing those coefficients that compromise data sparsity. Such a process can usually be improved by an elaborate statistical analysis of the dependencies between coefficients at different scales. Yet, while effective, traditional multi-resolution methods are designed to only remove one particular type of noise (e.g. Gaussian noise). Furthermore, only the input image is assumed to be given. Due to the unknown statistical properties of the noise introduced by the use of sprays, traditional approaches do not find the expected conditions, and thus their action becomes much less effective.

The proposed approach still performs noise reduction via transform space coefficient shrinkage, yet an element of novelty is introduced, in the form of partial reference images. Having a reference allows the shrinkage process to be data-driven. A strong source of inspiration were the works on the Dual-tree Complex Wavelet Transform by Kingsbury [13], the work on the Steerable Pyramid Transform by Simoncelli et al. [4], and the work on Wavelet Coefficient Shrinkage by Donoho and Johnstone [14].

The remainder of this paper is organized as follows. The Dual-tree Complex Wavelet Transform is introduced in Section II, while Section III outlines the concept of Random Spray sampling, and the image enhancement methods Random Spray Retinex and RACE. Section IV then presents the proposed denoising algorithm. The experimental setup and results are presented in Section V, and some final conclusions are drawn in Section VI.

II. Dual-Tree Complex Wavelet Transform

The Discrete Wavelet Transform (DWT) has been a founding stone for all applications of digital image processing: from image denoising to pattern recognition, passing through image encoding and more. While being a complete and (quasi-)invertible transform of 2D data, the Discrete Wavelet Transform gives rise to a phenomenon known as "checker board" pattern, which means that data orientation analysis is impossible. Furthermore, the DWT is not shift-invariant, making it less useful for methods based on the computation of invariant features.

In an attempt to solve these two problems affecting the DWT, Freeman and Adelson first introduced the concept of Steerable filters [15], which can be used to decompose an image into a Steerable Pyramid, by means of the Steerable Pyramid Transform (SPT) [4]. While, the SPT is an overcomplete representation of data, it grants the ability to appropriately distinguish data orientations as well as being shift-invariant. Yet, the SPT is not devoid of problems: in particular, filter design can be messy, perfect reconstruction is not possible and computational efficiency can be a concern.

Thus, a further development of the SPT, involving the use of a Hilbert pair of filters to compute the energy response, has been accomplished with the Complex Wavelet Transform (CWT) [16]. Similarly to the SPT, in order to retain the whole Fourier spectrum, the transform needs to be overcomplete by a factor of 4, i.e. there are 3 complex coefficients for each real one. While the CWT is also efficient, since it can be computed through separable filters, it still lacks the Perfect Reconstruction property.

Therefore, Kingsbury also introduced the Dual-tree Complex WaveletTransform (DTCWT), which has the added characteristic of Perfect Reconstruction at the cost of approximate shift-invariance [13].

Since the topic is extremely vast, only a brief introduction of the 2D DTCWT is given. The reader is referred to the the work by Selesnick et al. [17] for a comprehensive coverage on the DTCWT and the relationship it shares with other transforms.

The 2D Dual Tree Complex Wavelet Transform can be implemented using two distinct sets of separable 2D wavelet bases, as shown below.

$$\begin{aligned}
\psi_{1,1}(x,y) &= \phi_h(x)\psi_h(y), \quad \psi_{2,1}(x,y) = \phi_g(x)\psi_g(y), \\
\psi_{1,2}(x,y) &= \psi_h(x)\phi_h(y), \quad \psi_{2,2}(x,y) = \psi_g(x)\phi_g(y), \\
\psi_{1,3}(x,y) &= \psi_h(x)\psi_h(y) \quad \psi_{2,3}(x,y) = \psi_g(x)\psi_g(y)
\end{aligned} \tag{1}$$

$$\begin{aligned}
\psi_{3,1}(x,y) &= \phi_g(x)\psi_h(y), \quad \psi_{4,1}(x,y) = \phi_h(x)\psi_g(y), \\
\psi_{3,2}(x,y) &= \psi_g(x)\phi_h(y), \quad \psi_{4,2}(x,y) = \psi_h(x)\phi_g(y), \\
\psi_{3,3}(x,y) &= \psi_g(x)\psi_h(y) \quad \psi_{4,3}(x,y) = \psi_h(x)\psi_g(y)
\end{aligned} \tag{2}$$

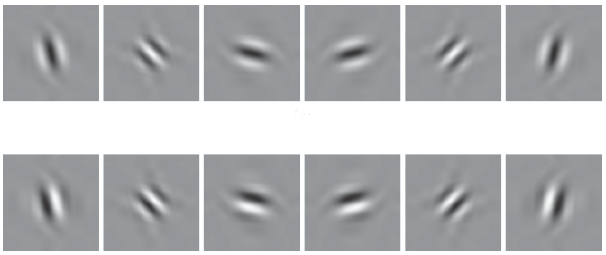

Fig. 1. Quasi-Hilbert pairs wavelets used in the Dual Tree Complex Wavelet Transform

The relationship between wavelet filters h and g is shown below

$$g_0(n) \approx h_0(n-1), \text{ for } j = 1 \tag{3}$$

$$g_0(n) \approx h_0(n-0.5), \text{ for } j > 1 \tag{4}$$

where j is the decomposition level.

When combined, the bases give rise to two sets of real, two-dimensional, oriented wavelets (see Fig. 1).

$$\psi_i(x,y) = \frac{1}{\sqrt{2}}\left(\psi_{1,i}(x,y) - \psi_{2,i}(x,y)\right) \tag{5}$$

$$\psi_i + 3(x,y) = \frac{1}{\sqrt{2}}\left(\psi_{1,i}(x,y) + \psi_{2,i}(x,y)\right) \tag{6}$$

$$\psi_i(x,y) = \frac{1}{\sqrt{2}}\left(\psi_{3,i}(x,y) + \psi_{4,i}(x,y)\right) \tag{7}$$

$$\psi_i + 3(x,y) = \frac{1}{\sqrt{2}}\left(\psi_{3,i}(x,y) - \psi_{4,i}(x,y)\right) \tag{8}$$

The most interesting characteristic of such wavelets is that they are approximately Hilbert pairs. One can thus interpret the coefficients deriving from one tree as imaginary, and obtain the desired 2D DTCWT.

Random Sprays abd two image enhancement algorithms that utilize them as sampling structures are introduced in the next Section.

III. RSR AND RACE

This Section, describes the process of Random Spray Sampling, then introduces Random Spray Retinex (RSR) and RACE (the fusion of RSR and ACE), two algorithms that utilize said sampling method.

A. Random Spray Sampling

Random Spray sampling was first introduced by Provenzi et al. [18]. Random sprays are an elaboration over the physical spatial scanning structure used by Land in his seminal work on Retinex [19]. In his experiments, Land used a structure resembling a set of paths departing from a central point, on which he mounted a number of photo-detectors.

Land's model gave rise to the path-wise family of Retinex algorithms [20], [21], which directly transposed Land's machinery into piece-wise linear paths used to scan the input image. A subsequent thorough mathematical analysis of Retinex [22] allowed the model to be significantly simplified, leading, in turn, to Random Sprays and RSR.

A single point of a random spray may be generated using the following formulation, and the whole spray is obtained by reiterating the process

$$\mathbf{p} = [\rho \cos(\theta), \rho \sin(\theta)] \tag{9}$$

where $\rho = \mathrm{rand}(0, R)$ and $\theta = \mathrm{rand}(0, 2\pi)$ and rand indicates the uniform random distribution. In particular, R is going to be set as the diagonal of the image, so that the spray can cover its entirety.

Each spray is then used to sample the image by transforming its points as follows

$$\tilde{\mathbf{p}} = \mathbf{p} + \mathbf{i} \tag{10}$$

where $\mathbf{i} = [i_x, i_y]$ are the coordinates of the pixel used as reference for sampling.

B. The problem of noise

According to the input image, the sharp sampling imposed by sprays leads to the introduction of speckle-like noise with an unknown distribution. The problem of noise has already been partially addressed in the work introducing RACE [23] by using a form of attachment to the original data, thereby strongly reducing the appearance of speckles in uniform areas. This process can be summarized by the following equation that is computed for each chromatic channel

$$\tilde{O}(x, y) = \beta(x, y) O(x, y) + (1 - \beta(x, y)) I(x, y) \tag{11}$$

where I indicates the input image, O is the output image of non-regularized RSR or RACE, and β is computed per-pixel. Given a specific spray k, the local parameter β is automatically determined for each chromatic channel

$$\beta_k(x, y) = (2\sigma_k(x, y))^{\frac{\sigma_{\min}}{\sigma_{\max}}} \tag{12}$$

where the quantities $\sigma_{\min}$ and $\sigma_{\max}$ are the image-wise standard deviations, while $\sigma_k(x, y)$ is the standard deviation for the spray in question.

However, the main problem with the above solution is that to reduce the appearance of noise the enhancement effect is also reduced.

IV. Proposed method

The main idea behind this work can be sumarized as follows: *highly directional content is what conveys the largest part of information to the Human Visual System*. This statement is backed up by past research, such as the Retinex theory as well as the high-order gray-world assumption (alias gray-edges) [24]. In particular, the local white patch effect described by Retinex comes into play when, for a given channel, the scanning structure samples a positive intensity change. For obvious geometrical reasons, intensity changes of a directional nature are more easily crossed (or sampled) than point-like structures such as noise.

Thus, following such an idea, the proposed method revolves around the shrinkage of the real wavelet coefficients generated by the Dual Tree Complex Wavelet Transform, according to data directionality.

Furthermore, since the HVS is highly sensitive to changes in luminance [25], the proposed method first converts the image in a space where the chroma is separated from the luma (such as YCbCr), and it operates on the wavelet space of the luma channel. While this may seem counter intuitive, since spray-based image enhancement algorithms usually operate per channel, the results show vast improvements without visible colour artefacts.

Finally, a fundamental assumption is made: the input image is considered to be either free of noise, or contaminated by non perceivable noise. If such an assumption holds, the input image contains the information needed for successful noise reduction.

The algorithm for the proposed method is given in Fig. 1. For ease of reference, a visual description is also given in Fig. 2. The following Subsections exmplain the details of the shrinkage process and the tests performed to optimize the algorithm parameters.

A. Wavelet coefficients shrinkage

Assuming level j of the wavelet pyramid, one can compute the energy for each direction $k \in \{1, 2, ..., 6\}$ as

$$e_{j,k} = (b^I_{j,k})^2 + (i^I_{j,k})^2 \tag{13}$$

Algorithm 1 Algorithm for proposed noise-reduction method.

$E_{RGB} \leftarrow \text{enhance}(I_{RGB})$

$I_{YCbCr} \leftarrow \text{rgb2ycbcr}(I_{RGB})$

$E_{YCbCr} \leftarrow \text{rgb2ycbcr}(E_{RGB})$

$b^I \leftarrow \text{dtcwt}(Y_I)$

repeat

  $b^E \leftarrow \text{dtcwt}(Y_E)$

  for $j = 1 \rightarrow J$ **do**

    for $k = 1 \rightarrow 6$ **do**

      $e_{j,k} \leftarrow \sum_k b^I_{j,k}$

    end for

    $w_j \leftarrow \text{mm}(\underset{k}{\text{stddev}}(e_{j,k}), \underset{k}{\text{median}}(e_{j,k}), \gamma_j)$

    for $k = 1 \rightarrow 6$ **do**

      $\tilde{b}^E_{j,k} \leftarrow w_j \cdot b^E_{j,k} + (1 - w_j) \cdot b^I_{j,k}$

      if $\text{ord}(b^E_{j,k}) \in \{1, 2\}$ **then**

        $b^O_{j,k} \leftarrow \tilde{b}^E_{j,k}$

      else

        $b^O_{j,k} \leftarrow b^I_{j,k}$

      end if

    end for

  end for

  $Y_E \leftarrow Y_O$

until $\text{ssim}(Y_I, Y_O) < 0.001$

$O_{YCbCr} = \text{concat}(Y_O, E_{CbCr})$

$O_{RGB} = \text{ycbcr2rgb}(O_{YCbCr})$

While coefficients associated with non-directional data will have similar energy in all directions. On the other hand, highly directional data will give rise to high energy in one or two directions (although this is not entirely true, as more than two directions may have high energy for "L" or "T" shaped features, but it does not compromise the efficacy of the proposed method).

The standard deviation of energy across the six directions $k = 1, 2, ..., 6$ is hence computed as a

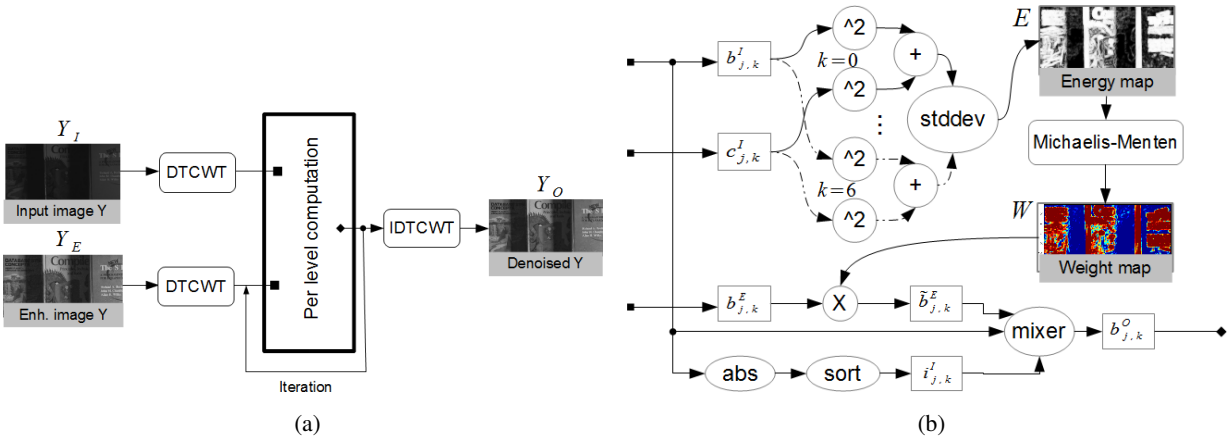

Fig. 2. Proposed method flowchart. (a) The luma channels of both the non-enhanced and the enhanced images are transformed using the DTCWT, and the obtained coefficients are elaborated. The output coefficients are transformed into the output image's luma channel via the inverse DTCWT. (b) The computation indicated by the box in (a) is performed per level of the decomposition. A directional energy map is first computed as the standard deviation of sum-of-squares of the coefficients. A weight map is then obtained by using the Michaelis-Menten function for normalization. The weight map is used to scale the real coefficients of the enhanced image.

measure of directionality.

$$e_j = \operatorname*{stddev}_k(e_{j,k}) \tag{14}$$

Obviously, the standard deviation is non-normalized and its range can vary widely. Thus, in order to make use of the computed data, the Michaelis-Menten function [26] is applied to normalize data range. The Michaelis-Menten function is a sigmoid-like function that has been used to model the cones responses of many species, making it a perfect candidate for the job. The equation is as follows:

$$\mathrm{mm}(x, \mu, \gamma) = \frac{x^\gamma}{x^\gamma + \mu^\gamma} \tag{15}$$

where x is the quantity to be compressed, γ a real-valued exponent and μ the data expected value (or its estimate).

A normalized map of directionally sensitive weights is obtained as

$$w_j = \mathrm{mm}(e_j, \operatorname*{median}_k(e_{j,k}), \gamma_j)$$

where the choice of γ depends on j as explained later on.

A shrunken version of the enhanced image's real coefficients, according to data directionality, is then computed as

$$\tilde{b}^E_{j,k} = w_j \cdot b^E_{j,k} + (1 - w_j) \cdot b^I_{j,k} \tag{16}$$

Since the main interested is retaining directional information, the output coefficients are computed according to Eq. 17

$$b^O_{j,k} = \begin{cases} \tilde{b}^E_{j,k}, \text{ if } \mathrm{ord}(b^E_{j,k}) \in \{1,2\} \\ b^I_{j,k}, \text{ if } \mathrm{ord}(b^E_{j,k}) \in \{3,4,5,6\} \end{cases} \tag{17}$$

where ord is the function that returns the index of a coefficient in $b^I_{k=1,2,\ldots,6}$ when the set is sorted in a descending order.

The meaning of the whole sequence can be roughly expressed as follows: where the non-enhanced image shows directional content, replace its two most significant coefficients with a (possibly) shrunken version from the enhanced image.

B. Parameter tuning

When dealing with functions with free parameters, a fundamental problem is finding the optimum paramter values. While this can often be attempted with optimization techniques, such methods are unfeasible in the case.

To at least provide a reasonable default value for γ_j, the parameter of the Michaelis-Menten function, and the depth of the complex wavelet decomposition J, three images from the USC-SIPI Image Database [27] were chosen. Such images provide a good mixture of mostly high-frequency detail (Mandrill), balanced high- and low-frequency content (Lenna), and mainly low frequency content (Splash). The chosen test images are shown in Fig. 7.

In different rounds, Gaussian, Poissonian and Speckle noise was added to the luma channel of said images and the proposed noise reduction method was run with 3 wavelet levels and values for γ_j varying from -5 to 10 in unit steps for the first and second levels of the decomposition. The value for γ_3 was fixed at 1, thereby reducing the Michaelis-Menten function to the Naka-Rushton formulation [28].

Since the decomposition depth is more dependent on the image than on γ_j, it was impossible to determine a single optimum value. Nonetheless, reasonable bounds were found to be $J_{min} = 1, J_{max} = 3$. Please note that J is the only parameter that needs to be set explicitly, since the variation in image quality can be extremely evident.

The performance was tested using the SSIM [29] measure, holding the unaltered luma channel as the absolute reference. Plots of the results are shown in Fig. 3. The iterations were stopped using a threshold of $t = 0.001$. The SSIM scores and PSNRs are both given in Table I.

For all the images the score improved for positive values of γ at all levels. Yet, the change is less

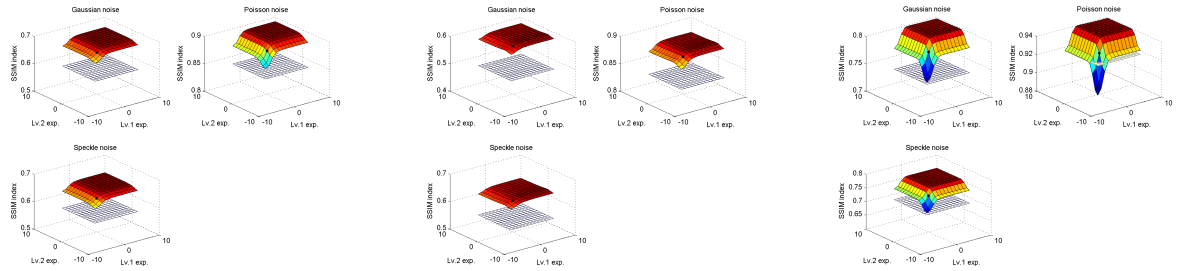

(a) (b) (c)

Fig. 3. SSIM plots for the chosen test images. The wireframe surface indicates the SSIM score obtained by the noisy image. The solid surface represents the SSIM score with respect to changing values of γ_j. The dark spot on the solid surface indicates the origin.

TABLE I

PSN RATIOS AND SSIM SCORES FOR TEST IMAGES FROM THE USC-SIPI IMAGE DATABASE.

		Noisy		Denoised	
Noise type	Img. name	PSNR	SSIM	PSNR	SSIM
Gaussian	Lenna	27.43	0.58	35.78	0.95
	Splash	27.68	0.49	36.37	0.93
	Mandrill	27.45	0.73	34.78	0.98
Poissonian	Lenna	30.33	0.84	35.78	0.95
	Splash	30.92	0.82	36.37	0.93
	Mandrill	30.16	0.91	34.78	0.98
Speckle	Lenna	27.07	0.55	33.96	0.94
	Splash	27.55	0.53	33.84	0.94
	Mandrill	26.96	0.69	33.87	0.97

sudden for $j = 1$. While non-optimal for all possible inputs, values of $\gamma_1 = 3$ and $\gamma_2 = 1$ represent a reasonable choice.

V. EXPERIMENTS

To test the proposed method, experiments were performed with three of the images originally used in the works on RSR [18] and RACE [23] which happened to trigger the undesired behaviour. The images, their noisy versions (RSR) and the noise reduced results by the proposed approach are all shown in Fig. 4.

The images shown in Figs. 7a - 7c were also modified to reduce the dynamic range and introduce a

(a) Book, original (b) Fire, original (c) Gallery, original

(d) RSR (e) RSR (f) RSR

(g) Denoised (h) Denoised (i) Denoised

Fig. 4. The proposed denoising method applied to RSR filtered images. The parameter J was set to 1 for *Book*, 2 for the other two pictures.

strong colour cast. The resulting images were used as test subjects, as illustrated in Fig. 7.

Finally, the proposed approach was compared to a recent development on the Non Local means approach by Buades et al. [30], namely the Foveated NL-means by Foi and Boracchi [31]. Three images were chosen from the said work, and the proposed noise reduction method used after the addition of Gaussian noise with varying standard deviation. The PSNRs and SSIM scores were both computed and are reported in Tables II and III: the numbers differ slightly from the original article since the images were generated anew. While the comparison is not entirely fair, as the Foveated NL-means is a reference-less denoising method, it clearly shows the advantage of assuming a partial reference.

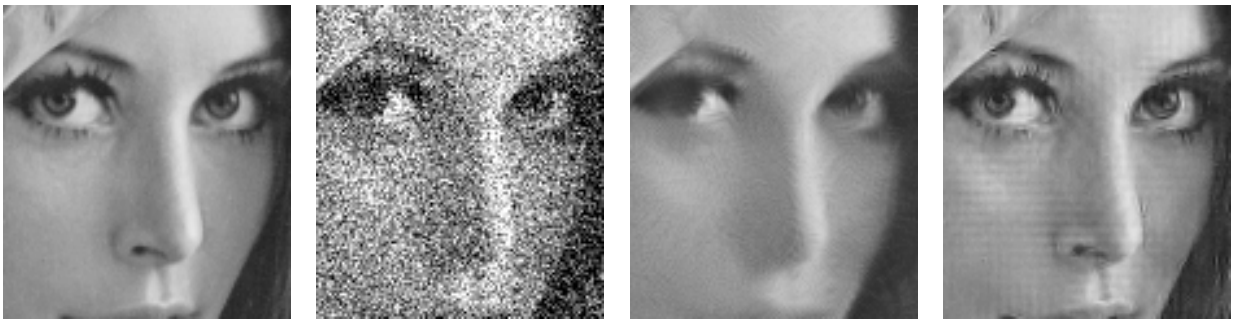

(a) Lenna, original (b) noisy, $\sigma = 50$ (c) Foveated NL-means (d) Proposed

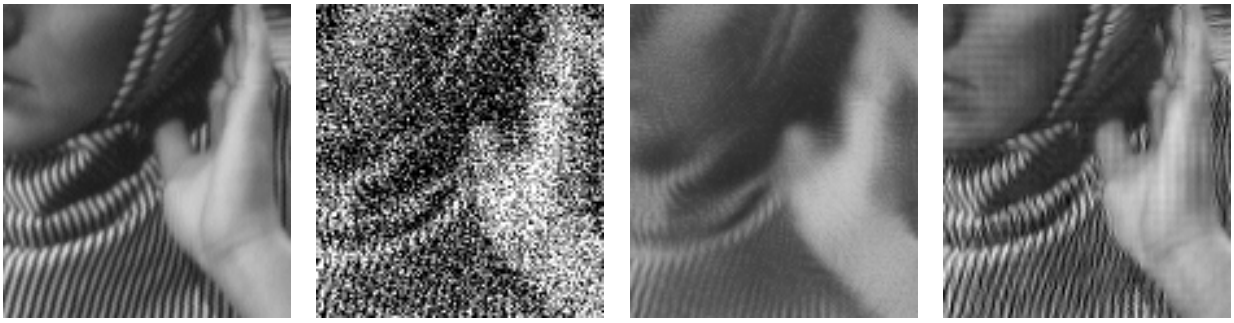

(e) Barbara, original (f) noisy, $\sigma = 70$ (g) Foveated NL-means (h) Proposed

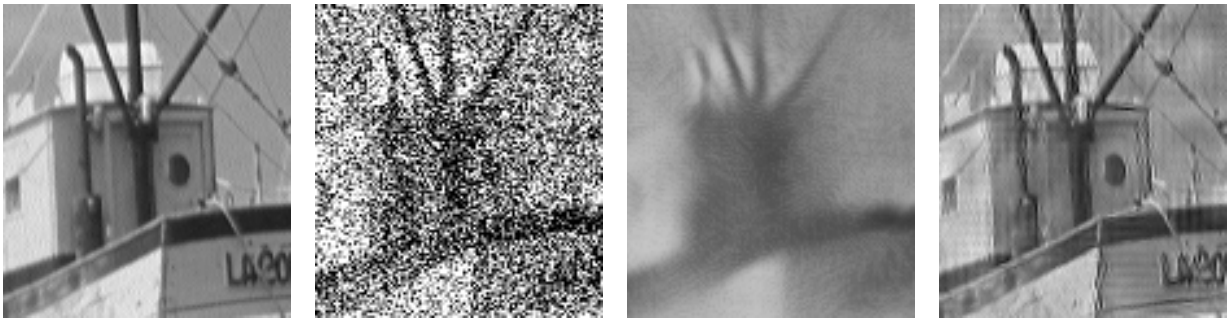

(i) Boats, original (j) noisy, $\sigma = 100$ (k) Foveated NL-means (l) Proposed

Fig. 5. Comparison between the proposed method and Foveated NL-means. Noise is Gaussian with standard deviation as per captions.

A. Scanline analysis

For a better analysis of the effects of the proposed denoising method, a scanline from two of the test images was selected with the objective of encompassing areas rich in detail, as well as "flat" ones.

The scanline data is plotted in Fig. 6a and 6b and on close inspection it becomes apparent how the proposed denoising method acted according to the desired behaviour.

In particular Fig. 4g shows how the cover of the blue book has been smoothed out, almost completely

TABLE II

COMPARISON OF PSNRS FOR THREE IMAGES TAKEN FROM THE WORK ON FOVEATED NL-MEANS.

	Barbara		Boats		Lenna	
σ	FNLM	Our	FNLM	Our	FNLM	Our
10	33.39	41.71	32.73	42.76	35.05	43.24
20	30.46	37.86	29.89	38.94	32.39	39.43
30	28.08	35.83	28.05	36.93	30.51	37.42
40	26.27	34.52	26.59	35.46	28.91	36.19
50	24.77	33.61	25.24	34.37	27.63	35.11
60	23.61	32.60	24.14	33.45	26.43	33.83
70	22.68	32.04	23.29	32.52	25.37	32.79
80	21.80	31.17	22.42	31.57	24.37	31.81
90	21.02	30.60	21.75	30.88	23.32	31.19
100	20.33	30.33	21.06	30.20	22.41	30.52

TABLE III

COMPARISON OF SSIM SCORES FOR THREE IMAGES TAKEN FROM THE WORK ON FOVEATED NL-MEANS.

	Barbara		Boats		Lenna	
σ	FNLM	Our	FNLM	Our	FNLM	Our
10	0.97	0.99	0.96	0.99	0.96	0.99
20	0.94	0.98	0.90	0.98	0.93	0.98
30	0.89	0.97	0.84	0.97	0.90	0.96
40	0.85	0.96	0.79	0.95	0.86	0.95
50	0.80	0.94	0.74	0.94	0.83	0.93
60	0.75	0.93	0.69	0.92	0.79	0.91
70	0.71	0.91	0.65	0.91	0.77	0.90
80	0.67	0.90	0.61	0.89	0.74	0.88
90	0.63	0.88	0.58	0.88	0.71	0.87
100	0.60	0.87	0.55	0.86	0.68	0.85

removing the noise, yet, at the same time, the letters in the title of the “red dragon” book are still sharp. The same is true for the rest of the text present in the image. This result is also indicative of how the proposed method relies on information present in the non-enhanced image, as the noise reduced output can deviate significantly from the enhanced input, whereas conventional methods will always be limited by the enhanced data.

Fig. 6b also shows a similar behaviour, as the small spikes present on the wall and parquet floor are

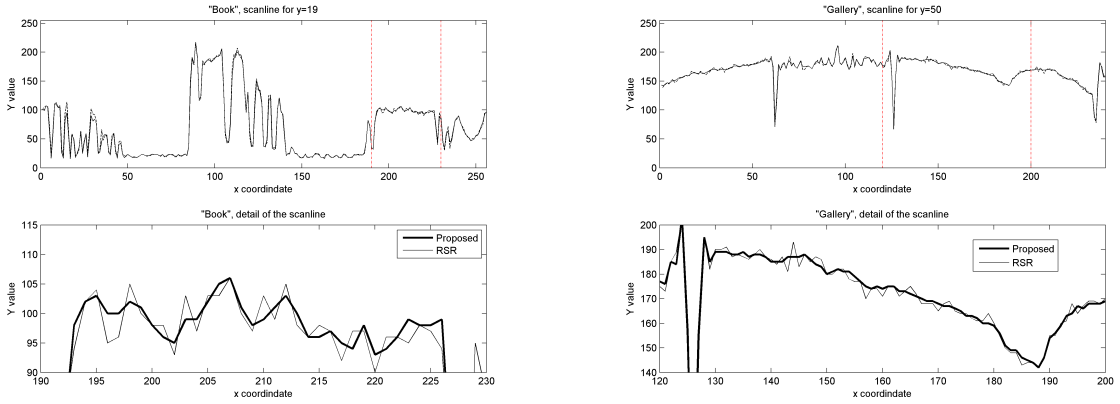

(a) (b)

Fig. 6. Scanline plots. The whole scanline is shown above, while below only a part of it is displayed, so that details become more apparent. The detail section extrema are indicated by discontinuous vertical lines in the topmost plot.

flattened, yielding a much more pleasant rendition of uniform surfaces. At the same time, highly detailed areas, such as the painting in the center of the image, are almost unaffected and retain all their visual appeal.

VI. Conclusions

This work presented a novel approach to noise reduction, especially point-wise noise. The proposed algorithm is expected to be applied as post-processing on the output of an image-enhancement method.

To achieve noise reduction, the proposed method exploits the data orientation discriminating power of the Dual Tree Complex Wavelet Transform, as well as the information contained in the non-enhanced image. Wavelet coefficient shrinkage and selection are then the basic mechanisms underlying the iterative processing. In contrast to other methods, the proposed approach requires no prior knowledge of the statistical properties of noise. The only explicitly required parameter is the depth of the DTCWT.

The performance was tested in three ways. First, noise with different statistical properties was added to images with a well known reference. The proposed approach was able to achieve great improvements in both the PSNRs and SSIM scores, regardless of the noise distribution.

The proposed approach was also compared to a recent development of the NL-means denoising algorithm, using images with a well known prior and Gaussian noise with varying standard deviation. The proposed method has shown consistent increases in PSNR by about 9 dBs on average, and produced higher SSIM scores that never dropped below 0.85.

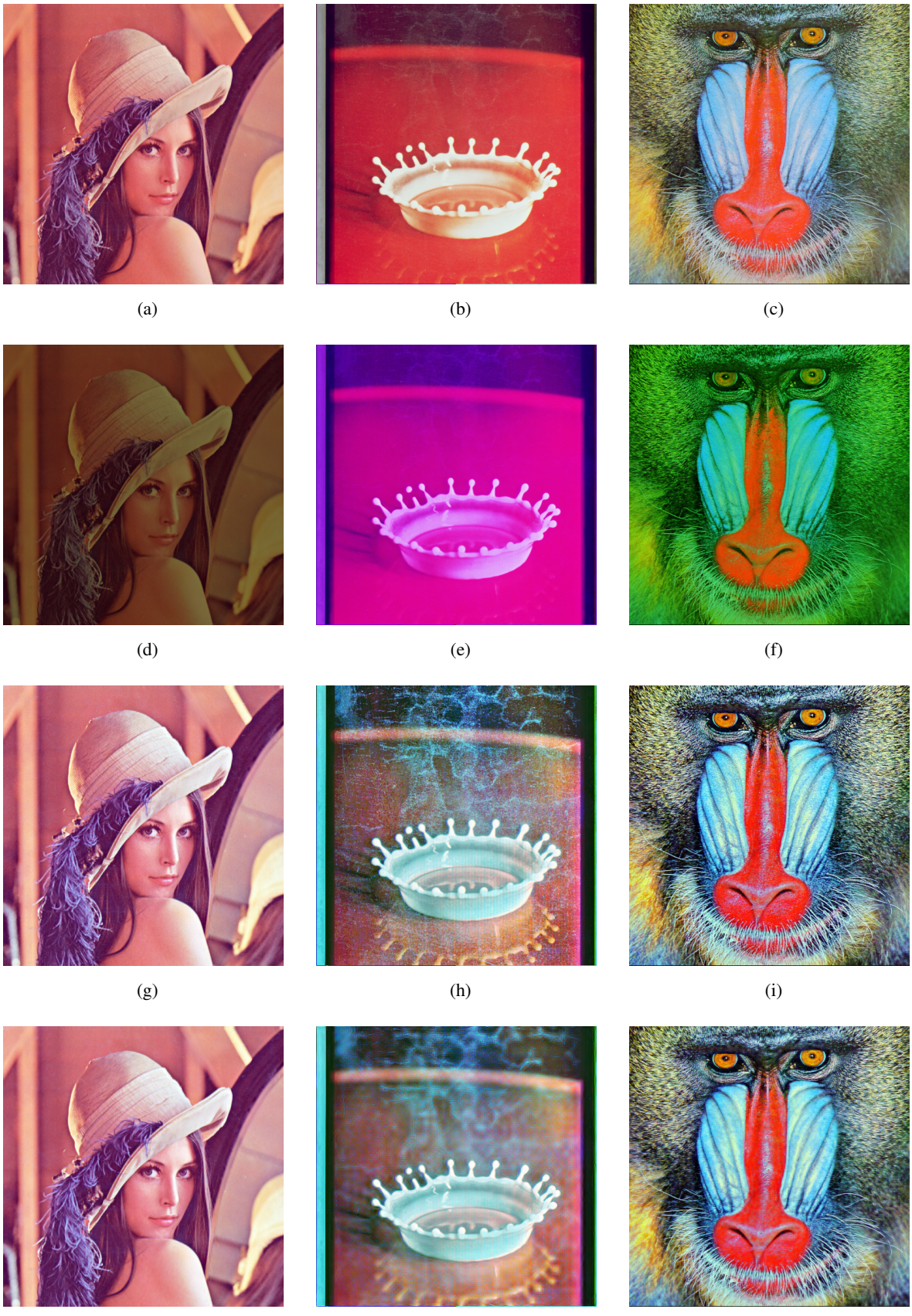

(a) (b) (c)

(d) (e) (f)

(g) (h) (i)

(j) (k) (l)

Fig. 7. Test images from the UCS-SIPI image database, results. *Lenna* was enhanced with RSR, while the others with the spray formulation of ACE. The noise reduction algorithm was run with $J = 3$ for images *Lenna* and *Splash*, and $J = 2$ for *Mandrill*.

The third batch of tests was performed using artificially degraded images with a well known reference, as well as images without a prior reference.

The proposed noise reduction method produced a good performance, removing noise without altering underlying structures most salient for human perception. However, the main limitations are the natural bounding of noise reduction due to the contrast of the non-enhanced image, and the appearance of patterning in the denoised image when the source is characterized by high levels of noise.

ACKNOWLEDGMENT

This work was supported by the Mid-career Researcher Program through NRF grant funded by the MEST (No. 2010-0000401).

REFERENCES

[1] H. A. Chipman, E. D. Kolaczyk, and R. E. McCulloch, "Adaptive bayesian wavelet shrinkage," *Journal of the American Statistical Association*, vol. 92, no. 440, pp. pp. 1413–1421, 1997. [Online]. Available: http://www.jstor.org/stable/2965411

[2] A. Chambolle, R. De Vore, N.-Y. Lee, and B. Lucier, "Nonlinear wavelet image processing: variational problems, compression, and noise removal through wavelet shrinkage," *Image Processing, IEEE Transactions on*, vol. 7, no. 3, pp. 319 –335, march 1998.

[3] D. Cho, T. D. Bui, and G. Chen, "Image denoising based on wavelet shrinkage using neighbor and level dependency," *International Journal of Wavelets, Multiresolution and Information Processing*, vol. 7, pp. 299–311, 2009.

[4] E. P. Simoncelli and W. T. Freeman, "The steerable pyramid: a flexible architecture for multi-scale derivative computation," in *2nd Annual International Conference on Image Processing*, 1995.

[5] F. Rooms, W. Philips, and P. Van Oostveldt, "Integrated approach for estimation and restoration of photon-limited images based on steerable pyramids," in *Video/Image Processing and Multimedia Communications, 2003. 4th EURASIP Conference focused on*, vol. 1, july 2003, pp. 131 – 136 vol.1.

[6] Hossein and Rabbani, "Image denoising in steerable pyramid domain based on a local laplace prior," *Pattern Recognition*, vol. 42, no. 9, pp. 2181 – 2193, 2009. [Online]. Available: http://www.sciencedirect.com/science/article/pii/S0031320309000077

[7] S. Foucher, G. Farage, and G. Benie, "Sar image filtering based on the stationary contourlet transform," in *Geoscience and Remote Sensing Symposium, 2006. IGARSS 2006. IEEE International Conference on*, 31 2006-aug. 4 2006, pp. 4021 –4024.

[8] W. Ni, B. Guo, Y. Yan, and L. Yang, "Speckle suppression for sar images based on adaptive shrinkage in contourlet domain," in *Intelligent Control and Automation, 2006. WCICA 2006. The Sixth World Congress on*, vol. 2, 0-0 2006, pp. 10 017 –10 021.

[9] K. Li, J. Gao, and W. Wang, "Adaptive shrinkage for image denoising based on contourlet transform," in *Intelligent Information Technology Application, 2008. IITA '08. Second International Symposium on*, vol. 2, dec. 2008, pp. 995 –999.

[10] Q. Guo, S. Yu, X. Chen, C. Liu, and W. Wei, "Shearlet-based image denoising using bivariate shrinkage with intra-band and opposite orientation dependencies," in *Computational Sciences and Optimization, 2009. CSO 2009. International Joint Conference on*, vol. 1, april 2009, pp. 863 –866.

[11] X. Chen, C. Deng, and S. Wang, "Shearlet-based adaptive shrinkage threshold for image denoising," pp. 1616 –1619, may 2010.

[12] J. Zhao, L. Lu, and H. Sun, "Multi-threshold image denoising based on shearlet transform," *Applied Mechanics and Materials*, vol. 29-32, pp. 2251–2255, 2012.

[13] N. G. Kingsbury, "The dual-tree complex wavelet transform: A new technique for shift invariance and directional filters," in *Proc. 8th IEEE DSP Workshop*, Aug. 912, 1998, p. Paper no. 86.

[14] D. L. Donoho and I. M. Johnstone, "Threshold selection for wavelet shrinkage of noisy data," in *Proc. 16th Annual Int. Conf. of the IEEE Engineering Advances: New Opportunities for Biomedical Engineers Engineering in Medicine and Biology Society*, 1994.

[15] W. Freeman and E. Adelson, "The design and use of steerable filters," *IEEE Trans. Pattern Anal. Mach. Intell.*, vol. 13, no. 9, pp. 891–906, September 1991.

[16] N. G. Kingsbury, "Image processing with complex wavelets," *Philos. Trans. R. Soc. London A, Math. Phys. Sci*, vol. 3570, no. 1760, pp. 2543–2560, 1999.

[17] I. W. Selesnick, R. G. Baraniuk, and N. G. Kingsbury, "The dual-tree complex wavelet transform: a coherent framework for multiscale signal and image processing," *IEEE Signal Process. Mag.*, vol. 6, p. 123151, 2005.

[18] E. Provenzi, M. Fierro, A. Rizzi, L. De Carli, D. Gadia, and D. Marini, "Random spray retinex: A new retinex implementation to investigate the local properties of the model," *IEEE Trans. Image Process.*, vol. 16, no. 1, pp. 162–171, 2007.

[19] E. Land and J. McCann, "Lightness and retinex theory," *J. Optical Soc. of America A*, vol. 61, pp. 1–11, 1971.

[20] D. Marini and A. Rizzi, "A computational approach to color adaptation effects," *Image and Vision Computing*, vol. 18, no. 13, pp. 1005–1014, 2000.

[21] A. Rizzi, D. Marini, and L. D. Carli, "Lut and multilevel brownian retinex colour correction," *Machine Graphics and Vision*, vol. 11, no. 2-3, pp. 153–168, 2002.

[22] E. Provenzi, L. D. Carli, A. Rizzi, and D. Marini, "Mathematical definition and analysis of the retinex algorithm," *J. Opt. Soc. Am. A*, vol. 22, pp. 2613–2621, 2005.

[23] E. Provenzi, C. Gatta, M. Fierro, and A. Rizzi, "A spatially variant white-patch and gray-world method for color image enhancement driven by local contrast," *IEEE Trans. Pattern Anal. Mach. Intell.*, vol. 30, no. 10, pp. 1757–1770, 2008.

[24] J. van de Weijer, T. Gevers, and A. Gijsenij, "Edge-based color constancy," *Image Processing, IEEE Transactions on*, vol. 16, no. 9, pp. 2207 –2214, sept. 2007.

[25] C. J. van den Branden Lambrecht, Ed., *Vision models and applications to image and video processing*. Kluwer Academic, 2001.

[26] L. Menten and M. I. Michaelis, "Die kinetik der invertinwirkung," *Biochem*, vol. 49, p. 333369, 1913.

[27] USC-SIPI image database. [Online]. Available: http://sipi.usc.edu/database/

[28] K. I. Naka and W. A. H. Rushton, "S-potential from colour units in the retina of sh (cyprinidae)," *Journal of Physiology*, vol. 185, pp. 536–555, 1966.

[29] Z. Wang, A. C. Bovik, H. R. Sheikh, and E. P. Simoncelli, "Image quality assessment: From error visibility to structural similarity," *IEEE Trans. Image Process.*, vol. 13, pp. 600–612, 2004.

[30] A. Buades, B. Coll, and J.-M. Morel, "A non-local algorithm for image denoising," in *Proc. IEEE Computer Society Conf. Computer Vision and Pattern Recognition CVPR 2005*, vol. 2, 2005, pp. 60–65.

[31] A. Foi and G. Boracchi, "Foveated self-similarity in nonlocal image filtering," in *Proc. IS&T / SPIE Electronic Imaging 2012*, 2012.

Massimo Fierro received his M.S. in Computer Science from the University of Milano, DTI in year 2007. He has since been working on his Ph.D. as a member of the Color & Imaging Laboratory at Kyungpook National University. His research intrests include HDR imaging, panoramic imaging, colour correction and image denoising.

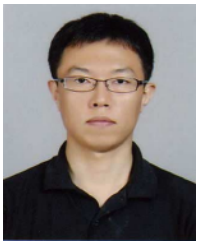

Ho-Gun Ha received his B.S. and M.S. degrees in Electrical Engineering & Computer Science from Kyungpook National University, Korea in 2007 and 2009, respectively. He has since been working on his Ph.D. as a member of the Color & Imaging Laboratory in Kyungpook National University. His research interests include image registration and colour image processing.

Yeong-Ho Ha received his B. S. and M. S. degrees in Electronic Engineering from Kyungpook National University, Taegu, Korea, in 1976 and 1978, respectively, and his Ph.D. degree in Electrical and Computer Engineering from the University of Texas at Austin, Texas in 1985. In March 1986, he joined the Department of Electronics Engineering of Kyungpook National University and is currently a professor. He has served as TPC chair, committee member, and organizing committee chair for many IEEE, SPIE, and IS&T international conferences, as well as and domestic ones. He served as the president and vice president of the Korean Society for Imaging Science and Technology (KSIST), and vice president of the Institute of Electronics Engineering of Korea (IEEK). He is a senior member of IEEE, a member of the Pattern Recognition Society and Society of IS&T and SPIE, and a fellow of IS&T and SPIE. His main research interests include in colour image processing, computer vision, and digital signal and image processing.